Buoyant melting instabilities beneath extending lithosphere: 2. Linear analysis

John W. Hernlund,[1,2] David J. Stevenson,[3] and Paul J. Tackley[1,4]

Received 18 November 2006; revised 18 October 2007; accepted 12 December 2007; published 8 April 2008.

[1] In a companion paper, numerical models reveal that buoyant melting instabilities can occur beneath extending lithosphere for a sufficiently small mantle viscosity, extension rate, and rate of melt percolation. However, in some cases, instabilities do not develop during extension but only occur after extension slows or stops. These results are suggestive of a critical behavior in the onset of these kinds of instabilities and motivate a linear analysis to study the onset of instability in a partially melting, passively upwelling plane layer of mantle beneath extending lithosphere. The model we employ includes the effects of buoyancy arising from thermal expansion, the presence of a retained fraction of partial melt, and depletion of the solid by melt extraction. We find a critical behavior in the onset of instability controlled by melt retention buoyancy that is characterized by a "Rayleigh" number M, such that M must exceed some critical value M_{crit} which depends on the efficiency of Stokes rise of a partially molten body relative to the rate of background percolation. Comparison of this theory to the numerical results in the companion paper yields a close quantitative agreement. We also find that solid depletion buoyancy can either stabilize or destabilize a partially melting layer, depending upon both the distribution of preexisting depletion and the magnitude of density changes with depth. This theory is compared with previous studies of buoyant melting instabilities beneath mid-ocean ridges where similar behavior was reported, and it suggests that the stability of passively upwelling, partially melting mantle underlying both narrow and wide rift settings is controlled by similar processes.

Citation: Hernlund, J. W., D. J. Stevenson, and P. J. Tackley (2008), Buoyant melting instabilities beneath extending lithosphere: 2. Linear analysis, *J. Geophys. Res.*, *113*, B04406, doi:10.1029/2006JB004863.

1. Introduction

[2] Upwelling fertile mantle beneath extending lithosphere may undergo decompression partial melting, and is the typical source of volcanism in most extensional provinces on Earth. Decompression melting of the upper mantle is associated with a decreased density due to the presence of a small fraction of melt and changes in composition and phase abundance in the residual solid rock. Thus if one portion of a partially melting layer ascends at a slightly faster rate, it may produce and retain more melt and as a consequence become less dense than adjacent portions of the layer. This in turn gives rise to a buoyancy surplus in faster upwellings that causes them to ascend even more quickly and produce more melt, thus setting the stage for a runaway instability. *Tackley and Stevenson* [1993] described the kind of instability arising from this scenario as "Rayleigh-Taylor-like," given its apparently unconditionally unstable behavior. This phenomenon has also been termed a "decompression melting instability" by *Raddick et al.* [2002].

[3] The tendency for such instabilities to develop in partially molten regions of Earth's mantle has been demonstrated in numerous numerical studies covering a variety of geological settings [e.g., *Parmentier and Morgan*, 1990; *Tackley and Stevenson*, 1993; *Jha et al.*, 1994; *Barnouin-Jha et al.*, 1997; *Schmeling*, 2000; *Choblet and Parmentier*, 2001; *Raddick et al.*, 2002]. However, in the companion paper by *Hernlund et al.* [2006] (hereinafter referred to as HTS), numerical models revealed that unstable buoyant convective motions in a plane layer of partially melting mantle beneath diffusely extending lithosphere do not always occur during extension, and in some cases may develop only after extension slows or stops. These behaviors were termed "synextensional" and "postextensional" according to whether instability set in during or after extension, respectively. Postextensional behavior is favored by a faster rate of extension, higher asthenospheric viscosity, and increased rate of melt percolation. The distinction

[1]Department of Earth and Space Sciences, University of California, Los Angeles, California, USA.
[2]Now at Department of Earth and Ocean Sciences, University of British Columbia, Vancouver, British Columbia, Canada.
[3]Division of Geological and Planetary Sciences, California Institute of Technology, Pasadena, California, USA.
[4]Now at Institute for Geophysics ETH-Zurich, Zurich, Switzerland.

0148-0227/08/2006JB004863$09.00

between these two behaviors was also found to depend on the depth distribution of solid depletion density changes, with the requirement that such effects must be significant at shallow levels of the partially molten zone in order to promote synextensional behavior.

[4] The results of HTS are thus suggestive of a critical behavior whereby some physical process is able to dampen the growth of instabilities during extension. Critical behavior of this type has also been proposed in previous studies of these kinds of buoyant melting instabilities within partially molten mantle beneath mid-ocean ridges [*Parmentier and Morgan*, 1990; *Jha et al.*, 1994; *Barnouin-Jha et al.*, 1997], in which the occurrence of instabilities related to decompression melting-generated buoyancy was found to depend on the spreading rate, viscosity, and rate of melt percolation in the same manner as the behavior found in HTS. Because the instability takes place in a plane layer of partially molten mantle in the latter study, it is apparent that this critical behavior results from fundamental physical processes within the layer instead of being attributable to any geometrical complexities present in the case of a mid-ocean ridge.

[5] Critical behavior in the dynamics of fluids occurs in a variety of scenarios [e.g., *Chandrasekhar*, 1961], where a perturbation to a preexisting state may either grow or decay depending upon the fluid's physical properties, externally imposed conditions and dimensions, as well as the nature (e.g., the magnitude and length scale) of the perturbation. In many situations a diagnostic parameter describing the propensity for instability may be used to assess whether or not unstable behavior is expected to arise in a given scenario, often by identifying a value for the relevant parameter corresponding to a state of marginal stability (i.e., at the locus of parameter space separating stable and unstable behavior). Familiar examples of significant geophysical importance are the critical Rayleigh number Ra_{crit} for the onset of thermal convection in a fluid containing a thermal gradient parallel to gravity, the critical Reynolds number Re_{crit} for the onset of turbulence in a laminar flow, and the critical magnetic Reynolds number Rm_{crit} for the sustenance of a magnetic field (i.e., dynamo action) in conducting fluids.

[6] The situation is complex in the present problem because up to three sources of buoyancy are present in partially melting mantle: thermal expansion buoyancy, buoyancy due to a retained fraction of melt, and buoyancy due to density changes in the solid residuum following melt extraction. Additionally, each of these buoyancy sources are subject to different transport properties, thus complicating a straightforward assessment of the essential physics of this process. HTS found that solid depletion buoyancy promotes synextensional instability only when solid density changes accompanying melting are present in the shallow portions of the partially melting layer. This is potentially important, because recent estimates by *Schutt and Lesher* [2006] suggest that density changes following melt depletion in spinel peridotite (appropriate for shallower melting of the asthenosphere) might be significantly smaller than previous estimates [e.g., *Oxburgh and Parmentier*, 1977; *Jordan*, 1979].

[7] The purpose of the present paper is to identify the individual roles that each source of buoyancy plays in the onset of convection in a passively upwelling and melting plane layer of mantle in order to gain a more clear understanding of the variety of behaviors observed in both the companion paper and in previous studies [*Parmentier and Morgan*, 1990; *Tackley and Stevenson*, 1993; *Jha et al.*, 1994; *Barnouin-Jha et al.*, 1997; *Schmeling*, 2000; *Choblet and Parmentier*, 2001; *Raddick et al.*, 2002]. The approach used here is to describe the appropriate basic state, subject it to a small perturbation, and then assess whether and how quickly instabilities would develop by solving the associated eigenvalue problem. We find that the critical behavior observed in previous studies is primarily due to a competition between melt retention buoyancy and percolation of melt up and out of the layer, and derive a "Rayleigh number" M for this process that depends on the rate of percolation and extension in addition to other properties of the melt and solid mixture. We also find that solid depletion buoyancy can only play a role in the onset of instability if the preexisting depletion gradient is smaller than adiabatic, which in the present context only occurs in shallower portions of the partially melting layer, thus explaining the necessity for significant solid density changes by melt extraction at shallower levels. Thermal convection instability, on the other hand, is less influential due to the buffering of lateral temperature changes by latent heat. We also compare the predictions of this analysis with the numerical results in the companion paper and the study of *Jha et al.* [1994], for which a good agreement suggests that this theory may be applied to the dynamics of partially melting mantle in a variety of rift settings on Earth, regardless of whether extension is narrowly or diffusely distributed.

2. Linear Analysis

[8] Here we examine the fate of a linear perturbation to the equations governing the creeping motion of a plane layer of asthenospheric mantle undergoing passive upwelling and partial melting as the result of diffuse extension. Although the basic state for the instability in this case is generally time-dependent, the relevant variables are considered to undergo an instantaneous linear perturbation relative to a temporarily fixed basic state in order to assess whether and how quickly the instability would proceed at any given time during the development and growth of a partially molten layer. In other words, the approach used here is to consider one-dimensional upwelling and melting in a plane layer up to a given time, taking a sort of "snap shot," and asking whether or not that state is stable or unstable with respect to small perturbations. This approach is analogous to the analysis of the onset of thermal (Rayleigh-Bènard-like) convection in a growing thermal boundary layer [e.g., *Schubert et al.*, 2001, and references therein]. In that purely thermal buoyancy-driven case, the thermal boundary layer thickness defines a characteristic length scale in the basic state and is generally an increasing function of time. However, the actual stability problem is performed upon a "snap shot" of the geotherm (taking advantage of its self-similarity) at a given time in the evolution and growth of the boundary layer, and the appropriate Rayleigh number is expressed in terms of the time-dependent boundary layer thickness. Thus the analysis only lends insight into whether the thermal boundary layer has grown to a sufficient thickness to permit convective instability. The linear analysis described below is conducted in the same spirit.

2.1. Mathematical Model

[9] We implement the same model as in HTS, which should be consulted for details. Here we only give a brief description of the model and the governing equations before proceeding to the linear analysis. In this model, the momentum balance is expressed in terms of an average (i.e., barycentric) velocity of melt and solid. Terms associated with resistance of the matrix to compaction are ignored. Melt percolation is modeled by a simple form of Darcy's law, and is solely driven by the isostatic pressure gradient. The relevant equations of motion are conservation of mass, momentum, the momentum difference between melt and solid phases, energy, melt fraction, and degree of solid depletion which are modeled by

$$\boldsymbol{\nabla}\cdot\mathbf{v}=0, \tag{1}$$

$$2\boldsymbol{\nabla}\cdot(\mu\boldsymbol{\nabla}\mathbf{v})+\boldsymbol{\nabla}\times(\mu\boldsymbol{\nabla}\times\mathbf{v})-\boldsymbol{\nabla}p=-\hat{z}(RaT+Rm\phi+Rd\zeta), \tag{2}$$

$$u\hat{z}=\phi(\mathbf{v}_m-\mathbf{v}_s)=\frac{Rm}{Mr}\phi^n\hat{z}, \tag{3}$$

$$\frac{\partial T}{\partial t}+\mathbf{v}\cdot\boldsymbol{\nabla}T=\nabla^2T-L\dot{m}, \tag{4}$$

$$\frac{\partial\phi}{\partial t}+\mathbf{v}\cdot\boldsymbol{\nabla}\phi=-\frac{\partial u}{\partial z}+\dot{m}, \tag{5}$$

$$\frac{\partial\zeta}{\partial t}+\mathbf{v}\cdot\boldsymbol{\nabla}\zeta=\frac{\partial(u\zeta)}{\partial z}+\dot{m}, \tag{6}$$

respectively, where $\boldsymbol{\nabla}$, $\mathbf{v}$, μ, p, $\hat{z}$, T, ϕ, ζ, L, u, $\mathbf{v}_m$, $\mathbf{v}_s$, and $\dot{m}$ are the gradient vector, bulk velocity (volume average of melt + solid velocity), bulk viscosity, nonisostatic pressure, upward unit vector, temperature, melt fraction, degree of solid depletion, latent heat, Darcy flux of melt through the solid, average melt velocity, average solid velocity, and melt production rate, respectively. Percolation is modeled according to porous Darcy flow driven solely by gravity with a permeability $k = k_0\phi^n$, where we choose $n = 2$ in order to simplify our analysis (we return to the general case in the discussion). The equations and variables have been nondimensionalized relative to a depth scale D, a thermal diffusion timescale D^2/κ, a temperature scale ΔT, a reference viscosity μ_0 and density ρ_0, resulting in the appearance of several nondimensional parameters:

$$Ra=\frac{\rho_0 g\alpha\Delta TD^3}{\kappa\mu_0}, \tag{7}$$

$$Rm=-\frac{gD^3}{\kappa\mu_0}\frac{\partial\rho}{\partial\phi}, \tag{8}$$

$$Rd=-\frac{gD^3}{\kappa\mu_0}\frac{\partial\rho}{\partial\zeta}, \tag{9}$$

$$Mr=\frac{\mu_m D^2}{\mu_0 k_0}, \tag{10}$$

where g, α, μ_m, and k_0 are the dimensional values of gravitational acceleration, thermal expansivity, melt viscosity, and reference Darcy permeability. Ra, Rm, and Rd are the respective "Rayleigh numbers" for temperature, melt, and solid depletion derived buoyancy. The quantity Mr is called a "melt retention" number, since it is inversely proportional to the rate of melt percolation, and more melt is retained in the matrix as Mr is increased.

[10] The meaning of the degree of solid depletion ζ can be understood by comparing equations (5) and (6). In the absence of melt percolation and segregation, $u \to 0$ and the governing equations for ϕ and ζ are identical. Thus ζ is equivalent to the cumulative volume fraction of melt that would be retained in the matrix in the absence of segregation (i.e., for batch melting), and measures the amount of melt extracted from the solid when $u > 0$. The melting model used here is a simple eutectic between two solid phases, one of which may or may not be relatively more dense than the other. The degree of melting ζ is assumed less than that for which one of the two solid phases would be entirely consumed, and therefore the temperature does not rise above the eutectic temperature T_s (which is assumed linear with depth), nor does the melt composition depart from the eutectic. This melting model is admittedly simplistic, however, addition of further details arising from more realistic phase equilibria is not yet justified given the complexity observed in the simplest models. The theory described in this paper can nevertheless be straightforwardly extended to more realistic mantle melting models in the future.

2.2. Basic State

[11] The basic state profiles for temperature T_0, depletion ζ_0, and melt fraction ϕ_0 are considered to be functions of time and depth only. The bulk upwelling velocity in the partially molten layer, v_0, is taken to be constant for simplicity; it is also independent of time t in this analysis. Under these restrictions, the basic state profiles are governed by the following set of equations:

$$u_0=\frac{Rm}{Mr}\phi_0^2, \tag{11}$$

$$\frac{\partial T_0}{\partial t}+v_0\frac{\partial T_0}{\partial z}=\frac{\partial^2T_0}{\partial z^2}-LFv_0, \tag{12}$$

$$\frac{\partial\phi_0}{\partial t}+v_0\frac{\partial\phi_0}{\partial z}=-\frac{\partial u_0}{\partial z}+Fv_0, \tag{13}$$

$$\frac{\partial\zeta_0}{\partial t}+v_0\frac{\partial\zeta_0}{\partial z}=Fv_0, \tag{14}$$

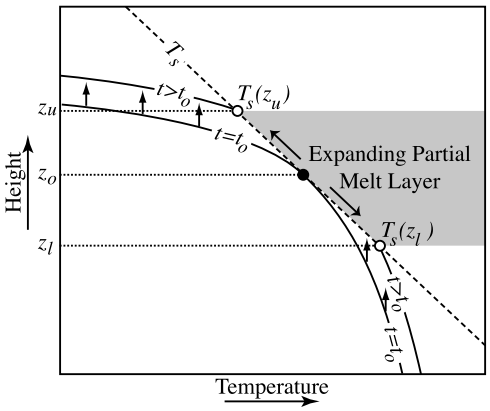

Figure 1. Schematic illustration of the scenario for the basic state, where an upwelling geothermal profile initially intersects the eutectic T_s at time $t = t_0$ and depth $z = z_0$, while continued upwelling at times $t > t_0$ leads to the expansion of a partially molten layer defined by the intersection of the geotherm at $z = z_l$ and $z = z_u$. Both z_l and z_u are therefore generally functions of time, such that $z_l = z_l(t)$ and $z_u = z_u(t)$.

where $u_0 = u(\phi_0)$ is the basic state Darcy velocity and F ($= \dot{m}/v_0$) is the nondimensional isentropic melt productivity for upwelling flow at the eutectic temperature T_s. In other words, upwelling of material a distance D along the eutectic would result in a degree of melting F. (Note that this quantity is often denoted as dF/dz in other studies; we instead use F for brevity.) Higher-order terms associated with the solid compaction flux have been omitted, allowing for simpler explicit expressions of the basic state profiles. Appropriate solutions to equations (12)–(14) will be developed below.

[12] Figure 1 shows the general scenario appropriate to the formulation of the basic state. For a curved geotherm, upwelling beneath a linear eutectic initially leads to intersection of the two curves at a single point $z = z_0$ at time $t = t_0$, while further upwelling allows the geotherm to intersect the eutectic at two different depths: the shallower depth is denoted z_u, while the deeper intersection is denoted z_l. In the region $z_l < z < z_u$ a partially molten region is formed that grows with time as upwelling proceeds further for $t > t_0$. In general, z_u and z_l are both functions of time (i.e., $z_u = z_u(t)$ and $z_l = z_l(t)$), because the curvature of the geotherm causes z_l to move downward and z_u to move upward from their initial intersection point (where $z_l(t_0) = z_u(t_0) = z_0$), although one or both of these intersections may saturate at limiting values if a well-developed quasi-steady upwelling layer is allowed to form at times $t \gg t_0$. The region $z_l < z < z_u$ will be the focus of the linear stability analysis, while variations in quantities above z_u or below z_l will usually be ignored except in the formulation of boundary conditions.

[13] According to the melting model adopted here, T_0 follows the eutectic temperature T_s throughout the partially molten layer, thus the basic state profile for temperature inside the partially molten layer is simply

$$T_0 = T_s. \tag{15}$$

It will be important later to recognize that equations (12) and (15) together require

$$dT_0/dz = dT_s/dz = -LF. \tag{16}$$

This relationship expresses the energy balance between latent heat absorption by melting and the decrease in temperature along the eutectic per unit distance of upwelling.

[14] The equation governing the partial melt profile (equation (13)) can be recast in the form

$$\frac{1}{v_0}\frac{\partial \overline{\phi}_0}{\partial t} + \left(1 + 2U_m\overline{\phi}_0\right)\frac{\partial \overline{\phi}_0}{\partial z} = 1, \tag{17}$$

where $\overline{\phi}_0 = \phi_0/F$ and $U_m = RmF/v_0Mr$. Taking $z = z(s)$ and $t = t(s)$ where s is a parametric variable, the characteristic equation belonging to equation (17) can be written as

$$\frac{d\overline{\phi}_0}{ds} = \frac{dt}{ds}\frac{\partial \overline{\phi}_0}{\partial t} + \frac{dz}{ds}\frac{\partial \overline{\phi}_0}{\partial z} = 1, \tag{18}$$

where comparison of like terms in equations (17) and (18) gives

$$\frac{dt}{ds} = \frac{1}{v_0} \tag{19}$$

and

$$\frac{dz}{ds} = 1 + 2U_m\overline{\phi}_0. \tag{20}$$

Equation (19) immediately gives $s = v_0t$, and integrating equation (18),

$$\overline{\phi}_0 = v_0(t + A). \tag{21}$$

Using this result to integrate equation (20),

$$z = U_m(v_0t)^2 + (1 + 2U_mAv_0)v_0t + B, \tag{22}$$

where A and B are constants that must be determined by specification of the boundary conditions. The lower boundary z_l of the partially molten layer generally moves downward in time according to

$$z_l = z_0 - f(t), \tag{23}$$

where $f(t)$ is a generic function of time such that $\dot{f}(t \geq t_0) \geq 0$ and $f(t = t_0) = 0$, where $\dot{f}$ is the derivative of f and t_0 is the time when the geotherm first intersects the eutectic (i.e., $z_l(t_0) = z_u(t_0) = z_0$). Consider the characteristic curve emanating from $z = z_l$ at time $t = t_c > t_0$. As a boundary condition, we require $\overline{\phi}_0 = 0$ on $z = z_l$. Equation (21) then gives

$$0 = v_0(t_c + A) \tag{24}$$

and $A = -t_c$ since $v_0 > 0$. Equation (22) then gives

$$B = z_0 - f(t_c) + U_m(v_0 t_c)^2 - v_0 t_c. \tag{25}$$

Combining equations (21), (22), and (25), the characteristic solution is then determined by

$$z - z_l(t) = f(t) - f\left(t - \overline{\phi}_0/v_0\right) + U_m\overline{\phi}_0^2 + \overline{\phi}_0. \tag{26}$$

Only for certain choices of $f(t)$ will it be possible to explicitly solve equation (26) for $\overline{\phi}_0$.

[15] The influence of the function $f(t)$ upon the partial melt profile in equation (26) is seen to depend upon the ratio $\tau_c = \overline{\phi}_0/v_0$, which is the characteristic time lag for equilibration between melt production and melt removal by percolation. In the context of the numerical models in the companion paper, $v_0 \approx 10^2$–10^3, $\phi_0 \approx 10^{-2}$, and $F \approx 0.2$ so that $\tau_c \approx 5 \times 10^{-4}$–$5 \times 10^{-5}$. In terms of dimensional units, for a layer of thickness 50 km and a thermal diffusivity of 10^{-6} m^2 s^{-1}, the effective time lag τ_c ranges between 40 ka and 400 ka, which should be compared with corresponding extension durations of about 2 Ma and 20 Ma, respectively. Thus we conclude that τ_c is negligibly small in the present context. In terms of ϕ_0 the basic state solution adopted (in the limit $\tau_c \to 0$) in the following linear analysis is then

$$\phi_0 = \frac{F}{2U_m}\left(\sqrt{1 + 4(z - z_l)U_m} - 1\right), \tag{27}$$

where again

$$U_m = \frac{RmF}{v_0 Mr}. \tag{28}$$

Differentiation of equation (27) at the base of the partially molten layer $z = z_l$ gives

$$\frac{d\phi_0}{dz}(z = z_l) = F, \tag{29}$$

which is generally valid independently of any previous approximations regarding τ_c. Since $\phi_0 = 0$ at the base of the partially molten layer, there is initially no percolation of melt as material enters the layer because all melt is retained in the limit $z \to z_l$ from above (and $\phi_0 \to 0$). Equation (29) therefore expresses that material at the very bottom of this layer (i.e., $z < 1/4\ U_m$) initially exhibits a simple linear melt profile where the increase in melt fraction with $z - z_l$ balances the melt produced per unit distance upwelling F. For $z > z_l$, this linear increase in ϕ_0 is accompanied by a stronger (quadratic) increase in u_0, and as a consequence the rate of percolation increases to the point where it balances melt production by transporting melt rapidly to the top of the layer.

[16] The basic state profile for depletion is generally a complicated function of the melting history of material throughout the partially molten layer. Here we will adopt the most general profile that can be constrained by the initial and boundary conditions without introducing additional degrees of freedom. From equation (14) we have

$$\frac{D\zeta_0}{Dt} = v_0 F, \tag{30}$$

where D/Dt is the material derivative. Equation (30) shows that ζ_0 is simply the cumulative (integrated) degree of melting experienced by a parcel of material as it upwells through the partially molten layer. As noted previously, the temperature in the partially molten region follows the eutectic temperature, and equations (12) and (14) may be combined to give (by equating $v_0 F$)

$$\frac{DT_0}{Dt} = \frac{DT_s}{Dt} = -L\frac{D\zeta_0}{Dt}, \tag{31}$$

which expresses the exchange of latent heat involved in increasing the degree of melting (or depletion) and the decrease in the temperature of a parcel of material as it undergoes decompression melting along the eutectic temperature. In a Lagrangian frame of reference moving with velocity $v_0\,\hat{z}$, equation (31) can be integrated to give

$$\zeta_0 = -L^{-1}\left[T_i + \frac{dT_s}{dz}(z - z_i) + g(z)\right], \tag{32}$$

where T_i is the temperature at which melting commenced at depth z_i for the ith solid parcel, and $g(z)$ in this context is a function that accounts for the history dependence of material originating in the partially molten layer at different depths. $g(z)$ can only be completely specified when the details of the interaction between a particular geotherm and the eutectic T_s are known. The case under consideration here is the intersection of a curved geotherm with a linear eutectic, whose equality at z_u and z_l requires that the depletion vanishes at z_u and z_l, yielding two basic boundary conditions. Instead of considering an error function profile used in the numerical models of this process, which leads to unnecessarily complicated expressions, a second-order series expansion is adopted for $g(z)$ of the form,

$$g(z) = Az^2 + Bz + C, \tag{33}$$

where A, B, and C are new constants unrelated to those given previously. Vanishing of ζ_0 at $z = z_l$ and $z = z_u$ yields two boundary conditions, however, according to equation (33), there are three constants to be determined. In order to be consistent with the description of the basic state partial melt profile ϕ_0, an additional boundary condition can be imposed by noting that the gradient of depletion at $z = z_l$ must be equal to that of the partial melt gradient at $z = z_l$ (where percolation is initially absent). In other words, where $u_0 = 0$, the governing equations for melt and depletion are identical, and given the same initial conditions should initially behave identically until ϕ_0 (and hence $u_0 \propto \phi_0^2$) becomes larger than infinitesimal. From equation (29), at $z = z_l$,

$$\frac{d\zeta_0}{dz} = \frac{d\phi_0}{dz} = F, \tag{34}$$

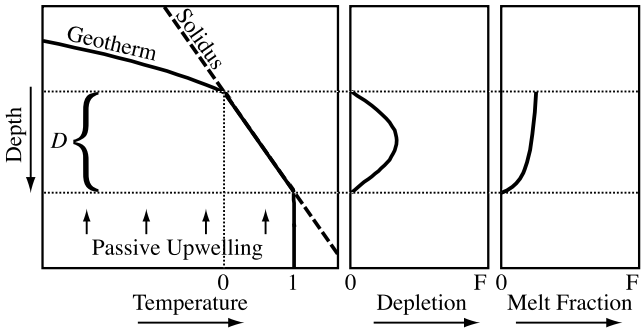

Figure 2. Summary of the basic state profiles for temperature, depletion, and melt fraction used in the linear analysis.

after which ζ_0 is given by

$$\zeta_0 = \frac{F}{z_u - z_l}(z_u - z)(z - z_l). \tag{35}$$

It is interesting to note that the second-order expansion in equation (33) together with the vanishing of ζ_0 at z_l and z_u implies that $z_l + z_u$ must be a constant, and therefore z_l moves downward at the same rate as z_u moves upward. Higher-order expansions for $g(z)$ would allow for a more general variation of both z_l and z_u, however, as noted above such an expansion is not completely constrained by the boundary conditions, and would therefore introduce additional (unwanted) parameters into the analysis.

[17] In the following sections, it will be convenient to choose $z_l = 0$ and $z_u = 1$ such that the dimensional length scale D of quantities appearing in the linear stability analysis (i.e., Ra, Rm, Rd, Mr, F, v_0, etc.) are scaled to the thickness of the partially molten layer. D is accordingly also a function of time in the basic state, however, as noted previously the linear analysis will be conducted only relative to fixed values of t and therefore D will also be considered to be temporarily fixed in order to evaluate whether the layer has attained an unstable state. The above assumptions made in defining the basic state allow each profile to be expressed in a form that scales in a simple way with the thickness of the partially molten layer rather than requiring a significantly different set of profiles as upwelling proceeds further. This is analogous to the manner in which the self-similarity of an error function geothermal profile is exploited in the Rayleigh-Bènard instability of a growing thermal boundary layer embedded in a half-space. Thus the basic state profiles for temperature, melt fraction, and depletion become

$$T_0 = T_s, \tag{36}$$

$$\phi_0 = \frac{F}{2U_m}\left(\sqrt{1 + 4zU_m} - 1\right), \tag{37}$$

$$\zeta_0 = Fz(1 - z). \tag{38}$$

The forms of these basic state profiles are illustrated in Figure 2.

2.3. Equations Governing the Perturbation

[18] As in the case of the onset of thermal convection [e.g., *Chandrasekhar*, 1961], the development of a decompression melting instability from the basic state is reduced to a linear eigenvalue problem by expanding a linear perturbation of the relevant variables into normal modes in the horizontal direction and finding solutions for the eigenvalues belonging to the fundamental eigenmodes as a function of the various control parameters and subject to appropriate boundary conditions. Let $\tilde{T}$, $\tilde{\phi}$, $\tilde{\zeta}$, and $\tilde{v}_z$ be linear perturbations relative to the basic state values T_0, ϕ_0, ζ_0, and v_0, which develop in the moving reference frame $v_0\hat{z}$, are periodic in a horizontal direction x, and grow or decay exponentially in time according to an instantaneous growth rate σ, i.e.,

$$\tilde{T} = T_0 + \Theta(z - v_0 t)\exp(ikx + \sigma t), \tag{39}$$

$$\tilde{\phi} = \phi_0 + \Phi(z - v_0 t)\exp(ikx + \sigma t), \tag{40}$$

$$\tilde{\zeta} = \zeta_0 + Z(z - v_0 t)\exp(ikx + \sigma t), \tag{41}$$

$$\tilde{v}_z = v_0 + V(z - v_0 t)\exp(ikx + \sigma t), \tag{42}$$

where k is the wave number of the periodic disturbance and $i = \sqrt{-1}$. Θ, Φ, Z, and V are the respective depth-dependent amplitudes of the perturbations to temperature, melt fraction, depletion, and vertical velocity. Note that the definition of k in section 2 is unrelated to the reference Darcy permeability, k_0.

[19] Upon substitution of the perturbations (39)–(42) into $\hat{z} \cdot \nabla \times \nabla \times$ equation (2), and equations (4), (5), and (6), ignoring terms of order higher than linear, and assuming a constant viscosity in the partially molten layer, the equations governing the perturbation are

$$\left(\frac{d^2}{dz^2} - k^2\right)^2 V = k^2(Ra\Theta + Rm\Phi + RdZ), \tag{43}$$

$$\left(\sigma - \frac{d^2}{dz^2} + k^2\right)\Theta = -V\left(LF + \frac{dT_0}{dz}\right), \tag{44}$$

$$\left(\sigma + c_0\frac{d}{dz}\right)\Phi = V\left(F - \frac{d\phi_0}{dz}\right), \tag{45}$$

$$\left(\sigma - \frac{d}{dz}u_0\right)Z = V\left(F - \frac{d\zeta_0}{dz}\right), \tag{46}$$

where

$$c_0 = \frac{du}{d\phi}_{\phi=\phi_0} = 2\phi_0\frac{Rm}{Mr}. \tag{47}$$

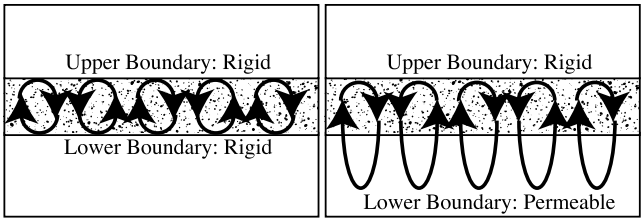

Figure 3. Illustration of the two kinds of boundary conditions considered in the linear analysis. In both cases, the upper boundary is immobile and rigid, while the lower boundary may be rigid or permeable to mantle flow.

Given appropriate boundary conditions, this set of equations may be solved to yield the growth rate σ. As usual, there is generally an infinite set of solutions belonging to different eigenmodes (i.e., Θ_n, Φ_n, Z_n, and V_n), each of which are associated with a different value for σ (i.e., σ_n). However, we will only be interested in the fundamental eigenmode that yields the largest values for $|\sigma|$, which is characterized by $V > 0$ for all z.

[20] Inserting the basic state value for dT_0/dz in equation (16) into equation (44),

$$\left(\sigma - \frac{d^2}{dz^2} + k^2\right)\Theta = 0, \tag{48}$$

and as a result, Θ is completely uncoupled from V. Therefore temperature plays no role in the onset of instability in this particular case, and we take $\Theta = 0$ for the remainder of this analysis. This decoupling is a consequence of the buffering of temperature to a melting trajectory in the basic state, which is imposed by the eutectic melting model adopted in this study.

[21] The influence of the basic state profiles ϕ_0 and ζ_0 upon the respective role of melt and depletion in the onset of instability can be understood by inspection of the right sides of equations (45)–(46). In particular, only differences between the vertical gradients in ϕ_0 or ζ_0 and F allows finite values for Φ or Z. This expresses the fact that only variations in each quantity relative to a simple adiabatic decompression melting profile can allow lateral variations to arise from this kind of perturbation, and is analogous to the requirement of a superadiabatic gradient for the onset of purely thermal convection.

2.4. Boundary Conditions

[22] The partially molten layer is considered to be overlain by a cool lithosphere of substantially higher viscosity. Although a small fraction of lithosphere might flow in response to stresses arising from buoyancy in the partially molten layer, it is treated as rigid for simplicity. Thus the vertical velocity perturbation V and the associated horizontal velocities vanish on the upper surface of the layer, and when combined with mass continuity this gives the boundary condition

$$V(z = 1) = \frac{d}{dz}V(z = 1) = 0. \tag{49}$$

The nature of the lower boundary can range from being essentially rigid to completely permeable to bulk flow depending on whether the viscosity of the partially molten layer is substantially lower than or equal to the underlying mantle viscosity. Both permeable and rigid lower boundary cases are treated here as end-members to bracket a range of possible behavior (see Figure 3). For a rigid lower boundary,

$$V(z = 0) = \frac{d}{dz}V(z = 0) = 0. \tag{50}$$

If the lower boundary is permeable to solid flow, the underlying mantle is considered to respond as a viscous half-space, and from equation (43) this passively driven flow is governed by

$$\left(\frac{d^2}{dz^2} - k^2\right)^2 V(z < 0) = 0. \tag{51}$$

The only solution to equation (51) which exhibits $V \to 0$ as $z \to -\infty$ is

$$V(z < 0) = (a_1 + a_2 z)\exp(kz), \tag{52}$$

where a_1 and a_2 are constants. The lower boundary conditions for the partially molten layer in the permeable case are determined by continuity of vertical velocity, horizontal velocity, tangential stress, and viscous traction (i.e., V is continuous to its third derivative) across $z = 0$ in accordance with equation (52):

$$V(z = 0) = a_1. \tag{53}$$

$$\frac{d}{dz}V(z = 0) = ka_1 + a_2. \tag{54}$$

$$\frac{d^2}{dz^2}V(z = 0) = k(ka_1 + 2a_2). \tag{55}$$

$$\frac{d^3}{dz^3}V(z = 0) = k^2(ka_1 + 3a_2). \tag{56}$$

The additional two conditions in the permeable lower boundary case constrain the values of a_1 and a_2. Another boundary condition arises by requiring the perturbations to temperature, melt fraction, and depletion to vanish at the base of the partially molten layer, for which equation (43) gives

$$\left(\frac{d^2}{dz^2} - k^2\right)^2 V(z = 0) = 0. \tag{57}$$

One final boundary condition would be needed for temperature because it is associated with a sixth-order differential eigenvalue problem, however, as noted above temperature plays no role in this analysis of the particular model considered in this study.

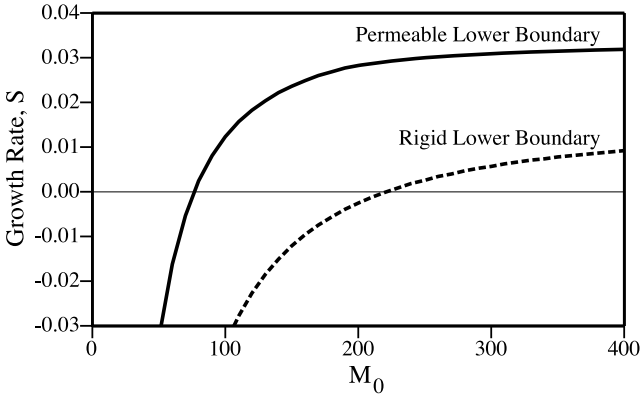

Figure 4. Results of the calculations for the normalized growth rate S as a function of M at a wave number of $k = k_{crit}$ when $M = M_0$ is a constant.

2.5. Partial Melt-Derived Buoyancy Only

[23] First, consider the end-member scenario where the establishment of a buffered temperature profile and a lack of density changes accompanying solid depletion leaves only the contribution of partial melt during the onset of instability. Combining equations (43) and (45), the perturbed circulation is governed by

$$\left(\frac{\sigma}{c_o}+\frac{d}{dz}\right)\left(\frac{d^2}{dz^2}-k^2\right)^2 V = k^2 M V, \tag{58}$$

where

$$M = \frac{Mr}{2\phi_0}\left(F - \frac{d\phi_0}{dz}\right). \tag{59}$$

For a given value of k, the profile M, and suitable boundary conditions, equation (58) may be solved for the growth rate σ, which will be positive if the perturbation grows, negative if it decays, and zero if it lies on the margin of stability. The basic state profile for ϕ_0 in equation (37) gives a depth-dependent function for M,

$$M = \frac{MrU_m}{\sqrt{4U_m z + 1}}, \tag{60}$$

the average value of which is

$$M_{avg} = \frac{Mr}{2}\left(\sqrt{4U_m + 1} - 1\right). \tag{61}$$

In terms of physical parameters, a good approximation for the average value of M when melt fractions are small (or $U_m \gg 1$) is

$$M_{avg} \approx \sqrt{\frac{\Delta\rho g F D^5}{\nu_0 \mu_0^2 (k_0/\mu_m)}}, \tag{62}$$

where F appearing in this expression is dimensional and $\Delta\rho$ is the density difference between melt and solid (i.e., $\Delta\rho = \rho_s - \rho_m$).

[24] As a reference, first consider the case where $M = M_0$ is a constant, which would only arise if ϕ_0 were approximately constant, giving $M \rightarrow M_0 = MrF/(2\phi_0)$. This approximation reduces the analysis to a simple linear eigenvalue problem that can be solved exactly. The depth-dependent M case is considered below using numerical solutions, and the results obtained here serve as a benchmark for those calculations. Substituting $\exp(qz)$ into equation (58), the characteristic roots q are governed by

$$\left(\frac{\sigma}{c_0}+q\right)\left(q^2-k^2\right)^2 - k^2 M_0 = 0, \tag{63}$$

and the solution for V in the partially molten layer is

$$V = \sum_{m=1}^{5} b_m \exp(q_m z), \tag{64}$$

where b_m are five constants and q_m are the five distinct roots of equation (63). Applying the boundary conditions to equation (64) and factoring out the constant coefficients b_m yields a matrix whose determinant must vanish to ensure the existence of a nontrivial solution.

[25] Solutions for the growth rate over a range of M_0 obtained by the above procedure are shown in Figure 4, where the results are given in terms of a normalized growth rate $S = \sigma/c_0 M_0$ for a single value of $k = k_{crit}$ (discussed below). S increases monotonically with M_0 from negative to positive values, and saturates as $M_0 \rightarrow \infty$. The maximum saturating values for S, denoted $S_{\max}$, are found to be (1) both boundaries rigid, $S_{\max} \approx 0.01453$ for $k \approx 4.57$, and (2) upper boundary rigid, lower boundary permeable, $S_{\max} \approx 0.03725$ for $k \approx 2.17$. The most interesting result is that M_0 is analogous to a "Rayleigh number," in that it must exceed some critical value (M_{crit}, say) in order for the instability to proceed (i.e., for $\sigma > 0$). Setting $\sigma = 0$ in equation (63), the variation of M_{crit} over a range of values for k at marginal stability is obtained and the results are shown in Figure 5. Defining k_{crit} to be the value of k that minimizes M_{crit} (i.e., M_0 when $\sigma = 0$), the solution procedure outlined above gives (1) both boundaries rigid, $M_{crit} \approx 220.7$ for $k_{crit} \approx 4.55$, and (2) upper boundary rigid, lower boundary permeable, $M_{crit} \approx 70.1$ for $k_{crit} \approx 2.20$. As usual, the critical number is smaller when one of the bounding surfaces is permeable, and the critical wave number is smaller by a factor of about two (i.e., the wavelength is longer). Note also that the wave number of the fastest growth rate is not very different from k_{crit}.

[26] The results obtained above for $M = M_0 =$ constant are only a crude approximation appropriate when $\phi_0 =$ constant, while M is generally depth-dependent as expressed by equation (60). In this case, the problem is more readily solved using numerical techniques. Equation (43) is discretized using second-order finite differences over n points within the partially molten layer, and equation (45) is integrated from the base of the partially molten layer using a second-order Runge-Kutta scheme. A solution to the resultant discrete equations is attained using relaxation in combination with a Newton-Raphson iteration for the desired eigenvalue [*Press et al.*, 1986]. The solutions obtained for $M = M_0 =$ constant are used to evaluate the accuracy of

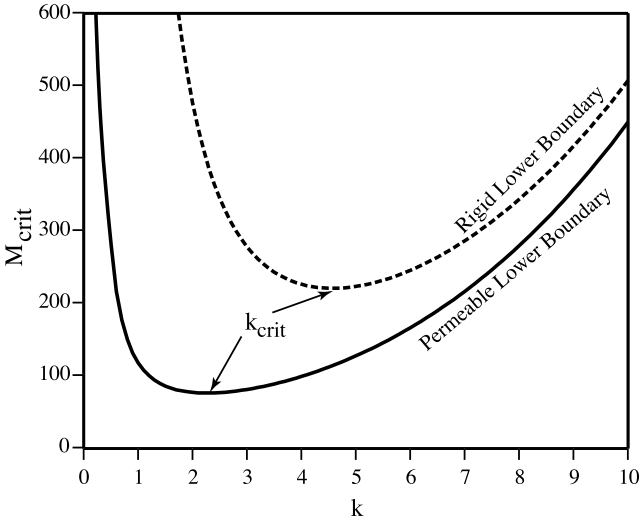

Figure 5. Results of the calculations for the value of M at the onset of instability as a function of wave number k. The dashed line represents the case where the lower boundary is rigid, and the solid line represents the case where the lower boundary is permeable, while the upper boundary is rigid in both instances.

the numerical solutions, and the relative errors in the critical values are found to be less than 0.2% for a grid density of $n = 64$, which is used in the following.

[27] Figure 6 shows the effects of depth-dependent M upon the value of M_{avg} determined at marginal stability ($\sigma = 0$) as a function of Mr. In both cases, the values are found to be within a few percent of the values for M_{crit} determined previously when $Mr > 100$. For a rigid upper and lower boundary, the value of M_{avg} increases slightly as $Mr \rightarrow 1$, while the opposite behavior is observed when the lower boundary is permeable. This may be attributed to the fact that larger values of M at the base of the layer imply that the propensity for instability is greatest at the base of the layer. When the lower boundary is rigid the perturbation in velocity is strongly suppressed at the bottom, while a permeable lower boundary allows for a nonzero velocity at $z = 0$, thus creating two different behaviors in the most unstable portion of the layer.

2.6. Effects of Buoyancy Asymmetry

[28] In the numerical modeling results of HTS, postextensional instabilities were observed to set in after a brief period of time following cessation or slowing of extension for a certain range of parameters. It is therefore interesting to consider what happens when extension stops (i.e., $v_0 \rightarrow 0$), and the melt produced by passive upwelling is allowed to drain from the partially molten layer. In this situation, $M \rightarrow \infty$, and one might expect that $S \rightarrow S_{\max}$. However, when no melt (or very little melt) initially exists, continued melting only occurs in upwellings while the downwellings remain unchanged. Physically, this kind of asymmetry means that downwelling flow is passively driven by adjacent buoyant upwellings, and the actual growth rate should be somewhat smaller than $S_{\max}$. Here we show that this asymmetry in the generation of buoyancy also complicates the simple periodic description of the perturbations, and leads to more localized upwelling flow.

[29] Consider the situation where only melt buoyancy is available to drive the instability and no melt is present (i.e., $\phi_0 = 0$). In this case, the perturbation equation governing Φ becomes (since $u_0 = c_0 = 0$)

$$\sigma\Phi = F\left(\frac{V + |V|}{2}\right). \tag{65}$$

When melting occurs only in upwellings, the right side of equation (65) effectively undergoes a transformation that is analogous to the effect of a diode upon an alternating electrical current (i.e., a half wave rectification). For a velocity field that varies like $\sin(kx)$, this rectification leads to an expanded Fourier series:

$$\sin(kx) \rightarrow \frac{1}{2}\sin(kx) + \frac{1}{\pi} + \frac{2}{\pi}\sum_{n=2,4,6,..} \frac{1}{n^2 - 1}\cos(nkx). \tag{66}$$

As a result, the horizontal variation in velocity cannot consist of a single mode, but is in general an infinite series of Fourier modes. This presents a problem because the Fourier components for melt are no longer linearly related to the velocity components in the equations governing the perturbation. The leading order term has a coefficient of 1/2, so that the right side of equation (65) becomes about half as large as the symmetric case, thus a crude approximation suggests the growth rate of the instability will be reduced by a factor of about two, i.e., $S \approx S_{\max}/2$.

[30] In order to obtain a better estimate of the effects of buoyancy asymmetry upon the growth rate and form of the circulation, we instead assume the vertical variation in V is known and solve for the appropriate horizontal variation under the effects of half wave rectification. As an example, consider a simple unit aspect ratio perturbed circulation with a dominant wave number $k = \pi$ and a vertical variation in velocity which goes like $\sin(\pi z)$. Let V_n be the amplitude of the velocity component that varies like $\exp(inkx)$. By

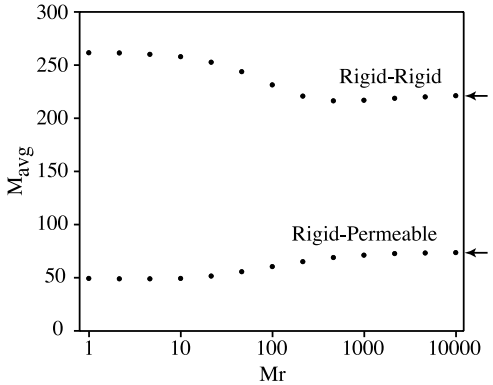

Figure 6. Results of the calculations for M_{avg} at marginal stability as a function of Mr for a wave number of $k = k_{crit}$ when M is taken to be depth-dependent. The arrows at right show the limiting values when M is taken to be constant for both cases.

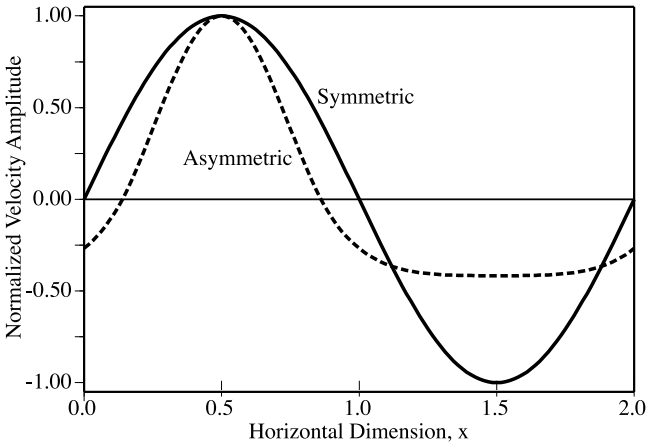

Figure 7. Effect of buoyancy asymmetry upon the normalized horizontal variation in vertical velocity for a simple unit aspect ratio circulation. Upwellings become more localized, while downwellings become broad and diffuse.

equating the various Fourier components in the momentum balance, one finds

$$V_n = \frac{RmF}{\sigma\pi^2}\frac{n^2}{(1+n^2)^2}V_n^a, \tag{67}$$

where V_n^a is the corresponding Fourier component of $(V + |V|)/2$. This can be solved numerically using discrete Fourier transforms as follows: Assume an initial velocity that goes like $\sin(\pi x)$, compute the Fourier components V_n^a of $(V + |V|)/2$, then calculate new velocity components using equation (67). Repeating this process recursively to convergence then yields the exact solution for all V_n. One finds that V_n is purely real (i.e., consisting of cosines) for even values of n, and is purely imaginary (i.e., consisting of sines) for odd n, and the first few components are $V_1 \approx 0.633$, $V_2 \approx -0.283$, $V_3 \approx -0.079$, $V_4 \approx 0.011$, $V_5 \approx -0.004$, $V_6 \approx 0.003$, while $V_n < 0.001$ for $n > 6$.

[31] The solution for the horizontal velocity variation obtained in this example is compared to the case where buoyancy is symmetric in Figure 7. The primary effect of asymmetry is to cause upwellings to become more localized, and downwellings to become slower and more diffuse. The converse would be true if buoyancy only developed in downwellings. The change in the growth rate under the effects of buoyancy asymmetry may also be computed, and is found to be about 3/5 the value of $S_{\max}$ in the corresponding symmetric case, which is a slightly smaller reduction than the factor of two estimated from the leading order term in equation (66).

2.7. Effects of Solid Depletion Buoyancy

[32] If undepleted mantle were introduced into a partially molten layer from below and subsequently carried upward adiabatically to the top, then by definition we would find that $d\zeta_0/dz = F$ such that the right side of equation (46) vanishes and Z and V become uncoupled. This would be true throughout the entire partially molten layer in a mid-ocean ridge-like setting, where material wells up through the entire partially molten layer from bottom to top. For the scenario considered here, the initial temperature profile contracts under the effects of extension and eventually intersects the eutectic temperature at two different depths (at the top and bottom of the partially molten layer). Because we assume the material which forms the partially molten layer is initially undepleted, the curvature of the geotherm causes the cumulative degree of melting in the middle of the layer to be more extensive than at the top or bottom, where ζ_0 necessarily vanishes. Note that in the basic state the lower portion of the partially molten layer is characterized by $d\zeta_0/dz = F$. The required curvature of the depletion profile in the upper portion of the layer, on the other hand, leads to a condition where $d\zeta_0/dz < F$. Thus the unstable part of the depletion gradient is near the top of the layer, which is where the right side of equation (46) obtains a nonzero value that can play a role in the momentum equation so long as $Rd > 0$ at the top of the layer (see Figure 8). However, if solid depletion buoyancy is only important in the deeper part of the layer and is negligible (i.e., $Rd = 0$) in the upper (unstable) part of the layer, then the potential for solid depletion to drive an instability is greatly diminished.

[33] To better quantify the role of solid depletion buoyancy in the onset of instability, consider the other limiting case $RdZ > 0$ and $Rm\Phi = 0$, so that only solid depletion-derived buoyancy initially drives the instability. Using equation (38) for ζ_0 leads to the following eigenvalue problem:

$$\left(\frac{d^2}{dz^2} - k^2\right)^2 V = k^2\frac{2RdF}{\sigma}zV, \tag{68}$$

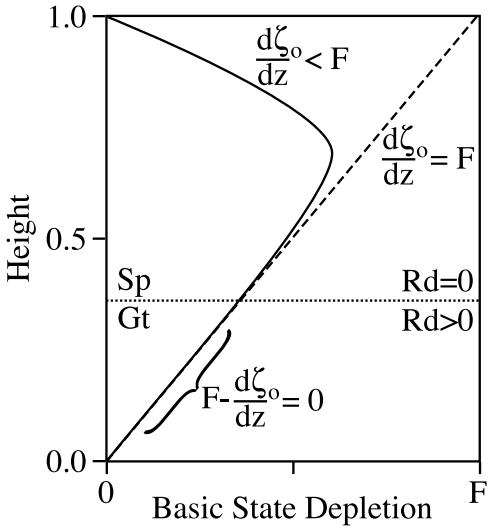

Figure 8. Schematic illustration of how the basic state depletion profile ζ_0 produced by extension alone is stable in the lower part of the layer (because $F - d\zeta_0/dz = 0$) and potentially unstable in the upper part of the layer (because $F - d\zeta_0/dz > 0$) if $Rd > 0$. However, in cases where the upper portion of the layer is in the spinel (Sp) stability field (Gt, garnet), the upper portion of the layer has $Rd = 0$, and in this case, there is no effective buoyancy derived from depletion at the onset of instability.

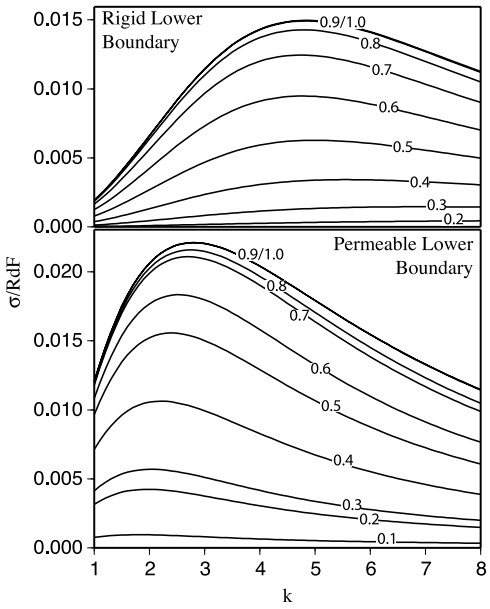

Figure 9. Growth rate of the solid depletion buoyancy-driven instability (curves) for different values of z_{sp} (labels on curves).

where the solid compaction advection term $u_0 Z$ is ignored. In this case, no marginal states are possible and the perturbation within the partially molten layer grows unconditionally. The appearance of a factor of z on the right-hand side of equation (68) illustrates that the propensity for depletion driven instability is strongest at the top of the layer where the unstable depletion gradient is present.

[34] To obtain a solution for the growth rate in this case, V can be expanded into a power series of the form

$$V = \sum_{n=0}^{N} c_n z^n \tag{69}$$

and truncated at degree N. Substituting this expression into equation (68) leads to the following recursion relation for the constants c_n:

$$(1+n)(2+n)(3+n)(4+n)c_{n+4} - 2k^2(1+n) \cdot (2+n)c_{n+2} + k^4 c_n - k^2 \lambda c_{n-1} = 0, \tag{70}$$

where $\lambda = 2RdF/\sigma$. This recursion in combination with the boundary conditions results in a set of equations, and upon factoring out the constants c_n yields a $(N-1) \times (N-1)$ matrix whose determinant must vanish to ensure the existence of a nontrivial solution. This yields an approximate solution for λ as a function of k, which approaches the exact solution as N is increased sufficiently ($N > 30$) as a consequence of the strong order of convergence. The maximum growth rates in this case are found to be (1) both boundaries rigid, $\sigma \approx 0.0150RdF$ for $k_{\max} \approx 4.82$, and (2) upper boundary rigid, lower boundary permeable, $\sigma \approx 0.0221RdF$ for $k_{\max} \approx 2.80$. For comparison, if one adopts $d\ln\rho/d\zeta = 6\%$ and $d\ln\rho/d\phi = 15\%$ (as in HTS), then the growth rate for solid depletion-derived buoyancy alone is about five times smaller than the maximum growth rate for partial melt-derived buoyancy alone. Also, the fastest growing wave number for depletion-derived buoyancy is slightly higher than in the case where only melt-derived buoyancy is important.

[35] Finally, we examine the effects of a garnet-spinel transition occurring inside the layer at a height $0 \le z_{sp} \le 1$, such that $Rd = 0$ in the shallower spinel stability field for $z \ge z_{sp}$ and $Rd > 0$ in the deeper garnet stability field for $z < z_{sp}$. This represents the extreme case where density changes accompanying depletion in the spinel stability field are negligible in comparison to changes in the garnet stability field [*Schutt and Lesher*, 2006]. The eigenvalue problem in this case is given by

$$\left(\frac{d^2}{dz^2} - k^2\right)^2 V = k^2\left[1 - \Gamma\left(z - z_{sp}\right)\right]\frac{2RdF}{\sigma} zV, \tag{71}$$

where Γ is the Heaviside function such that $\Gamma(z - z_{sp}) = 0$ for $z < z_{sp}$ and $\Gamma(z - z_{sp}) = 1$ for $z \ge z_{sp}$. This is solved by the shooting method for a variety of values for $0 \le z_{sp} \le 1$ (the results for $z_{sp} = 1$ are the same as obtained above by power series expansion). Figure 9 shows the results for the growth rate as a function of k, illustrating the fact that the deeper the buoyancy is distributed in the layer, the slower the rate of growth of the instability. The near coincidence of the curves for $z_{sp} = 0.9$ and 1 as well as the smaller suppression of growth rates in the lower permeable boundary cases illustrate the additional influence of rigid boundary conditions. A change in preferred (i.e., fastest growing) wave number can also be seen as z_{sp} assumes smaller values.

3. Discussion

[36] Several general conclusions can be arrived at based on the foregoing linear analysis: (1) the "Rayleigh number" M must be greater than the critical value M_{crit} during extension in order to manifest instabilities driven by partial melt buoyancy and (2) solid depletion buoyancy must be significant at shallower levels of the partially molten layer in order to exert a significant destabilizing influence in the onset of instability. It is also apparent that the growth rate for the instability must be significantly greater than unity (measured in units of the thermal diffusion time) in order for instabilities to develop before conductive cooling of the layer extinguishes the partially molten region, consistent with the assumptions made regarding the basic state. Below we discuss the conformity of the linear stability analysis with the numerical modeling results in HTS, the physical interpretation of the existence of a critical Rayleigh number M_{crit}, and a reexamination of previous studies of decompression melting instabilities beneath mid-ocean ridges in light of the results of this study.

3.1. Comparison of the Linear Analysis to Numerical Results

[37] The ability of the linear results obtained above to adequately explain the results of the numerical calculations in HTS can be evaluated quantitatively. The thickness of the partially molten layer D and the average upwelling velocity

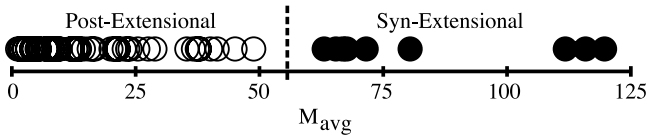

Figure 10. Distribution of M_{avg} during extension calculated from the numerical results of HTS for cases where depletion buoyancy is unimportant in the shallower portion of the model domains, showing that the transition from postextensional (open circles) to synextensional (solid circles) instability is well captured using M_{avg} as a diagnostic measure. The nonuniform distribution of points is a consequence of the nonlinear mapping of model parameters into M_{avg}.

v_0 are straightforwardly measured in the numerical models, allowing quantities such as Rm and Mr to be rescaled and thus permitting a straightforward calculation of M_{avg}. For the upwelling velocity, which was considered a constant in the linear analysis, the average value of $\mathbf{v} \cdot \hat{z}$ in the partially molten layer is used. Following this procedure, one finds that the distinction between "synextensional" and "postextensional" instability is well explained by a critical value of M_{avg} (see Figure 10). The highest value of M_{avg} for a postextensional result is 48.9, while the lowest value of M_{avg} for a synextensional result is 62.8, implying that $48.9 < M_{crit} < 62.8$. This is within the range of $M_{avg} \approx 50-70$ at marginal stability determined in the linear analysis when the lower boundary is permeable, which is most appropriate for comparison because there is no rigid lower boundary at the base of the partially molten layer in the numerical models.

[38] In the numerical results of HTS in cases where depletion buoyancy was strong everywhere in the model domain, a finite degree of circulation was always observed prior to the cessation of extension, and the bimodal behavior seen in the spinel and mixed phase cases was not apparent. Although this type of scenario cannot be addressed fully using linear analysis, the foregoing results suggest a relatively simple explanation for this kind of behavior. Depletion-related buoyancy can lead to an unconditionally unstable scenario beneath extending lithosphere if some of the material at the top of the layer is less depleted than material in the middle of the layer, an effect that is created by intersection of a curved geotherm with a linear eutectic as discussed previously. Here we estimated that an instability driven solely by depletion buoyancy grows more slowly (by about a factor of five) than a purely melt-driven instability. In any case, the enhanced instability caused by depletion buoyancy in the upper part of the partially molten layer thus provides a sort of "jump start" for the growth of the instability, which likely enhances the occurrence of synextensional instabilities. However, the ability for partial melt to act in concert with depletion-derived buoyancy and enhance this flow is still subject to the suppressing effects of background percolation, which is also evident at finite times in results of HTS for the dependence of erupted melt volume upon the Darcy coefficient k_0/μ_m.

[39] Cases found in HTS with only a weak or no instability can be understood as the consequence of either (1) a long growth time that is comparable to or smaller than the effective thermal diffusion time of the partially molten layer or (2) a rate of circulation due to the instability which is smaller than the rate of passive upwelling due to extension. In the first scenario, thermal conduction of heat from the layer upward into the overlying lithosphere causes it to cool and freeze before significant unstable motions are able to develop. In the second case, there is a slightly increased melt production rate in upwelling portions of the instability and a compensatory decrease in melt production in downwelling portions of the instability such that the net effect upon total melt production is nil.

3.2. Physical Meaning of the Rayleigh Number M

[40] In Rayleigh-Bénard thermal convection the Rayleigh number Ra is often interpreted in terms of a ratio between the timescale of Stokes rise of a thermal plume and its thermal diffusion timescale. Here we show that an analogous treatment for partial melting in a rising Stokes body yields similar insights into the physical meaning of the critical phenomenon found in the full stability analysis. Additionally, we note that the foregoing analysis was performed assuming that the Darcy permeability k follows a power law relationship of the form $k = k_0\phi^n$ with $n = 2$. This assumption allowed for explicit expressions that would be considerably more cumbersome in the general case. However, the appropriate value of n for melt migration in Earth's mantle is poorly constrained. Here we allow for other values of n in order to evaluate the more general case.

[41] The rate of rise of a buoyant partially molten body through a fluid is given by a Stokes-like formula of the form

$$v_{st} = \frac{A\Delta\rho g \phi_{st} D^2}{\mu}, \tag{72}$$

where $\Delta\rho$ is the density difference between solid and melt, D is now the characteristic dimension of the body, g is the acceleration of gravity, μ is the effective viscosity of the surrounding material through which the buoyant body ascends, and ϕ_{st} is the characteristic or average fraction of melt inside the body (internal variations are ignored here). A is a dimensionless constant that depends on the geometry of the body and the influence of its surroundings (for a sphere of diameter D in an infinite medium $A = 1/18$).

[42] The fraction of melt maintained in the rising body ϕ_{st} is determined by a balance between the rate of melt production Fv_{st} and the rate of removal by upward melt percolation,

$$Fv_{st} = \frac{B\Delta\rho g k}{\mu_m D} = \frac{B\Delta\rho g k_0 \phi_{st}^n}{\mu_m D}, \tag{73}$$

where B is a dimensionless geometric constant of order unity. Combining these expressions, we obtain

$$\phi_{st}^{n-1} = \frac{AF\mu_m D^3}{Bk_0\mu}, \tag{74}$$

and for the Stokes velocity

$$v_{st} = \Delta\rho g \left(\frac{A}{\mu}\right)^{n/(n-1)} \left(\frac{\mu_m F}{k_0}\right)^{1/(n-1)} D^{(2n+1)/(n-1)}. \tag{75}$$

For $n = 2$ these results are very similar to the scaling analysis given in HTS.

[43] Now consider a layer of Stokes bodies rising together side-by-side under some external influence with vertical velocity v_0. Initially, none are rising faster than the rest, since the density of their surroundings is the same, and the imposed rate of upwelling is uniformly distributed among them. The equilibrium between melt production and percolation is given (as before) by

$$v_0 = \frac{B\Delta\rho g k_0 \phi_0^n}{F\mu_m D}. \tag{76}$$

Suppose that some of the bodies attempt to rise a bit faster than their neighbors by an amount v' and thereby support an extra fraction of melt ϕ' according to

$$v_0 + v' = \frac{Bk_0\Delta\rho g(\phi_0 + \phi')^n}{F\mu_m D} \tag{77}$$

and try to profit from an excess buoyant ascent rate

$$v' = \frac{A\Delta\rho g\phi' D^2}{\mu}, \tag{78}$$

due to the enhanced decompression melting rate and retained melt. In order for the difference in rise rates to be self-sustaining we require $\phi' > 0$. To find out whether this is possible we combine the above expressions, expand $(\phi_0 + \phi')^n$, cancel balanced terms containing only v_0 and ϕ_0 by equation (76), and divide by ϕ' to obtain

$$\begin{aligned}\phi_{st}^{n-1} - n\phi_0^{n-1} &= \phi_{st}^{n-1} - \left(\frac{dk}{d\phi}\right)_{\phi=\phi_0} \\ &= \phi'\left[\frac{n(n-1)}{2}\phi_0^{n-2} + ..\right] > 0.\end{aligned} \tag{79}$$

The condition $\phi' > 0$ becomes

$$M' = \left[\left(\frac{\Delta\rho g}{v_0}\right)^{n-1}\frac{F\mu_m D^{2n+1}}{\mu^n k_0}\right]^{1/n} > M'_{crit} = \frac{nB^{1/n}}{A}, \tag{80}$$

where M' is the characteristic "Rayleigh number" for this case and M'_{crit} is the critical value that M' must exceed in order for the instability to proceed. For the case $n = 2$, M' can be written as

$$M' = \sqrt{\frac{\Delta\rho g F\mu_m D^5}{\mu^2 v_0 k_0}}, \tag{81}$$

which can be seen to be exactly the same expression as the one for M_{avg} derived from the full stability analysis in equation (62). When $n = 3$, the appropriate formulation of M' is

$$M' = \left[\left(\frac{\Delta\rho g}{v_0}\right)^2\frac{F\mu_m D^7}{\mu^3 k_0}\right]^{1/3}. \tag{82}$$

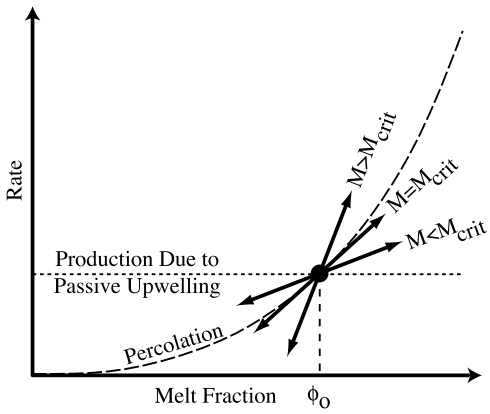

Figure 11. Illustration of the meaning of the critical number M_{crit}. The basic state consists of a balance between melt production and melt percolation (solid circle) from which point the perturbation takes place. In order for the instability to proceed, the buoyant circulation must support a larger melt fraction in upwellings than in downwellings, which can only occur if the melt fraction grows at a rate which is faster than percolation. Three kinds of perturbations are shown to illustrate the relationship between percolation and buoyant melt production according to whether M is less than, equal to, or greater than M_{crit}.

We can obtain a basic order of magnitude estimate for M'_{crit} by assuming $A = 1/18$ (for a sphere in an infinite medium) and $B = 1$, in which case $n = 2$ gives $M'_{crit} = 36$ and $n = 3$ yields $M'_{crit} = 54$. For material ascending just beneath high-viscosity lithosphere, this value for A is an upper bound on the rise rate efficiency, so we expect that in geophysically relevant cases M'_{crit} should be larger, in good agreement with the full linear stability analysis.

[44] The criteria $\phi_{st}^{n-1} > (dk/d\phi)_{\phi}=\phi 0$ for instability suggests the following simple physical interpretation: differences in buoyant rise rates in an upwelling layer of partially melting material can only be maintained if the fraction of melt supported by buoyant rise is greater than can be accommodated by an increased rate of percolation alone (see Figure 11). We also notice that M_{crit} can be interpreted as the ratio of the power law index for Darcy permeability n and the efficiency of Stokes rise A.

3.3. Preferred Wavelength of Circulation

[45] Intimately associated with the value of M_{crit} (or alternatively $S_{\max}$) is a preferred lateral length scale (or wavelength) for circulation defined by k_{crit} (or $k_{\max}$). Note that numerical models have shown that the wavelength of this kind of circulation can be dependent upon variable viscosity [*Choblet and Parmentier*, 2001], which is not considered in the present linear analysis. An additional complication is that the effective perturbation for any sublithospheric instability can be strongly influenced by preexisting heterogeneity. Abrupt changes in deep-rooted lithospheric structure (e.g., at the edge of a craton) may be a more relevant determinant in controlling the location of buoyant melting instabilities in some settings [*Raddick et al.*, 2002]. In the context of a "snap shot" basic state it is also important to note that a system passing from $M < M_{crit}$ to $M > M_{crit}$ will initially tend to develop instabilities with a

dimensional wavelength $2\pi D_i/k_{crit}$, where D_i is the thickness of the layer at the onset of instability. However, because the thickness of the layer can still increase following the onset of instability, the persistence of this initial unstable length scale at later times would lead to an apparently smaller wavelength relative to the thickness D_f of the layer at later times. This kind of apparent blue-shifting effect (by an amount D_f/D_i) will be most significant for synextensional instabilities, as postextensional behavior is characterized by $D_i = D_f$. The possibility for this kind of history dependence means that caution must be used when attempting to apply preferred horizontal length scales to observations.

3.4. Mid-ocean Ridges

[46] An interesting application of the theory outlined in this paper is the potential occurrence of buoyant melting instabilities in partially molten mantle beneath mid-ocean ridges. Unstable convective flow beneath ridges will inevitably affect melt production rates along the ridge, which in turn may exert a strong control upon the modes of deformation observed near ridge axes [e.g., *Buck et al.*, 2005]. It has been suggested that unstable flows beneath mid-ocean ridges, either as Rayleigh-Taylor instabilities resulting from accumulation of low-density melt [e.g., *Whitehead et al.*, 1984; *Crane*, 1985] or as small-scale thermal convection [e.g., *Rabinowicz and Briais*, 2002], might control the length scales of ridge segmentation. Buoyant instabilities beneath slow spreading mid-ocean ridges such as in the Mid-Atlantic are also suggested by the observation of pronounced gravity lows in the centers of some ridge segments [e.g., *Lin et al.*, 1990]. While it is not entirely clear whether the enhanced three-dimensional structure associated with slow spreading ridges (relative to fast spreading ridges) is a cause or consequence of buoyant instabilities in the underlying mantle, a necessary condition is the ability for instabilities to develop in an otherwise two-dimensional setting [*Parmentier and Morgan*, 1990].

[47] In three-dimensional models including the effects of solid depletion buoyancy, *Parmentier and Morgan* [1990] introduced a periodic temperature perturbation from below the ridge axis and found a transition between two-dimensional and three-dimensional structure as spreading rate is decreased. This unstable flow is characterized by a flow vorticity parallel to the direction of plate spreading and a corresponding change in melt productivity along the ridge axis. The scenario they studied is somewhat different than the buoyant melting instability considered in this study because lateral variations in depletion in their model were induced by shifting the depth of onset of melting downward in locations of higher temperature. According to the analysis performed in the present study, such an effect is probably necessary for depletion buoyancy to become important because purely internal stability of a plane layer (in the absence of melt retention buoyancy) requires a preexisting depletion gradient that is less than adiabatic (i.e., $d\zeta_0/dz < F$), while ridges are best characterized by adiabatic decompression melting (i.e., $d\zeta_0/dz = F$).

[48] Three-dimensional modeling studies of the mid-ocean ridge scenario by *Jha et al.* [1994] and *Barnouin-Jha et al.* [1997] including the effects of partial melt buoyancy and melt migration by Darcy percolation found similar behavior. For lower values of viscosity, rates of melt percolation and spreading rates, buoyant melting instabilities were found to occur inside the partially molten region beneath the ridge (termed "on-axis" instabilities), while for other ranges of parameters unstable flow only occurred away from the ridge axis (termed "off-axis" instabilities) or not at all. Thus these results revealed three types of scenarios: on-axis, off-axis, and no instability. Although there exist potentially important differences between the basic setting for development of melt buoyancy-driven instabilities beneath mid-ocean ridges and diffusely extending lithosphere, the behavior observed for mid-ocean ridges is quite analogous to the behavior found in HTS if we identify "synextensional" with "on-axis" instabilities, and "postextensional" with "off-axis" instabilities. This is because the mantle beneath a ridge axis is undergoing passive upwelling and background melting (similar to synextensional conditions), while material transported laterally away from the ridge axis in the plate spreading direction is no longer actively upwelling and as a consequence the melt drains out of the layer as it begins to cool to subsolidus temperatures (similar to postextensional conditions).

[49] Figure 12 shows the results for the occurrence of on-axis instabilities as a function of mantle viscosity and spreading rate for two different values of the Darcy coefficient k_0/μ_m from the study of *Jha et al.* [1994], with a line drawn in each case for M_{avg} = constant from the results of this study. The fit is good in predicting the basic dependence of on-axis instability upon the parameters, though not perfect (one case in each set is not well fit). The estimated value of M_{avg} obtained using the half spreading rate for v_0 and other values cited in the study is about 10–20, suggesting that the critical value of M for a mid-ocean ridge scenario may be several times smaller than that for instability in a plane layer.

4. Conclusion

[50] The results of the present linear analysis demonstrate that the critical behavior for the onset of instability driven by melt retention buoyancy observed in previous studies is due to a competition between melt percolation and the rate of growth of buoyant circulation driven primarily by melt retention buoyancy. A newly found "Rayleigh number for this process was derived that accurately predicts whether instabilities occur in numerical models of this process in a plane layer of passively upwelling mantle. The results are in good agreement with studies of this process beneath mid-ocean ridges, suggesting that this same kind of critical behavior in the onset of buoyant decompression melting instabilities is important in a wide variety of rift settings, regardless of whether extension is narrowly or diffusely distributed. The role of solid melt depletion variations in destabilizing a partially melting layer is sensitive to the depth distribution of density changes and the preexisting gradient in depletion.

[51] As a final note, it is important to keep in mind when applying this theory that the parameters appearing in the Rayleigh number M are not all generally independent of one another. This is particularly true of k_0 and n, where an increased value of one must be accompanied by an increase

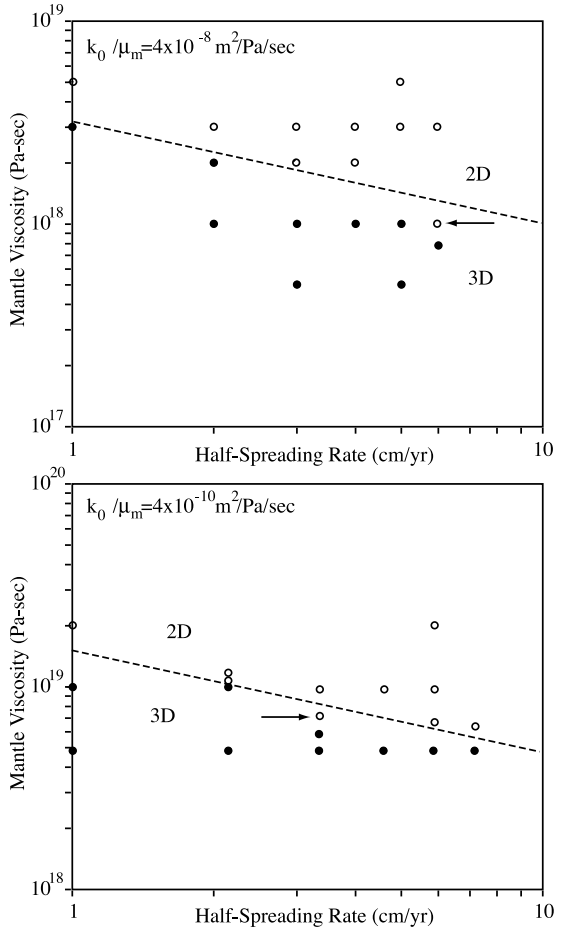

Figure 12. Results taken from the study of *Jha et al.* [1994] showing the regime boundary between 2-D (open circles) and 3-D structure (solid circles) in models of a mid-ocean ridge that included melt retention and depletion buoyancy. Here, ''3D'' means cases where instabilities were seen to develop at the ridge, while ''2D'' means that no instabilities were observed beneath the ridge. In each diagram, a phase boundary is plotted (dashed line) for each case at a constant value of $M \approx 20$. In each plot, a result that is not fit by the present theory is indicated by an arrow.

in the other in order to maintain similar Darcy velocities for a given melt fraction. Furthermore, rapid extension in some settings can be associated with high deviatoric stress, leading to nonlinear behavior in the rheology of the underlying mantle. In such a case, the effective viscosity of a partially molten layer could become a strongly decreasing function of v_0. This opens the possibility that the role of μ_0 in the Rayleigh number M can become inverted for high values of v_0 if the nonlinearity in rheology is sufficiently strong.

[52] **Acknowledgments.** Reviews of preliminary versions of this material by Abby Kavner and Gerald Schubert greatly improved this manuscript. We are grateful to Paul H. Roberts for thorough reviews and contributions to the mathematical presentation of the linear stability analysis. Reviews by Todd Bianco and Justin Revenaugh were also helpful in improving the clarity and substance of this manuscript. Discussions with William B. Moore, Lee Bargatze, and Don Anderson were also helpful. This work was supported in part by the NSF CDYEL project and a grant from IGPP Los Alamos.

References

Barnouin-Jha, K., E. M. Parmentier, and D. W. Sparks (1997), Buoyant mantle upwelling and crustal production at oceanic spreading centers: On-axis segmentation and off-axis melting, *J. Geophys. Res.*, *102*, 11,979–11,990.

Buck, W. R., L. L. Lavier, and A. N. B. Poliakov (2005), Modes of faulting at mid-ocean ridges, *Nature*, *434*, 719–723.

Chandrasekhar, S. (1961), *Hydrodynamic and Hydromagnetic Stability*, Clarendon Press, Oxford, U. K.

Choblet, G., and E. M. Parmentier (2001), Mantle upwelling and melting beneath slow spreading centers: Effects of variable rheology and melt productivity, *Earth Planet. Sci. Lett.*, *184*, 589–604, doi:10.1016/S0012-821X (00)00330-7.

Crane, K. (1985), The spacing of rift axis highs: Dependence upon diapiric processes in the underlying asthenosphere, *Earth Planet. Sci. Lett.*, *72*, 405–414.

Hernlund, J. W., P. J. Tackley, and D. J. Stevenson (2006), Buoyant melting instabilities beneath extending lithosphere, 1. Numerical models, *J. Geophys. Res.*, doi:10.1029/2006JB004862, in press.

Jha, K., E. M. Parmentier, and J. P. Morgan (1994), The role of mantle-depletion and melt-retention buoyancy in spreading-center segmentation, *Earth Planet. Sci. Lett.*, *125*, 221–234.

Jordan, T. H. (1979), Mineralogies, densities and seismic velocities of garnet lherzolites and their geophysical implications, in *The Mantle Sample: Inclusions in Kimberlites and Other Volcanics, Proceedings of the Second International Kimberlite Conference*, vol. 2, edited by F. R. Boyd and H. O. A. Meyer, pp. 1–14, AGU, Washington, D. C.

Lin, J., G. M. Purdy, H. Schouten, J.-C. Sempere, and C. Zervas (1990), Evidence from gravity data for focused magmatic accretion along the Mid-Atlantic Ridge, *Nature*, *344*, 627–632.

Oxburgh, E. R., and E. M. Parmentier (1977), Compositional and density stratification in the oceanic lithospherecauses and consequences, *J. Geol. Soc. London*, *133*, 343–354.

Parmentier, E. M., and J. P. Morgan (1990), Spreading rate dependence of three-dimensional structure in oceanic spreading centres, *Nature*, *348*, 325–328.

Press, W. H., S. A. Teukolsky, W. T. Vetterling, and B. P. Flannery (1986), *Numerical Recipes: The Art of Scientific Computing*, Cambridge Univ. Press, New York.

Rabinowicz, M., and A. Briais (2002), Temporal variations of the segmentation of slow to intermediate spreading mid-ocean ridges 2. A three-dimensional model in terms of lithosphere accretion and convection within the partially molten mantle beneath the ridge axis, *J. Geophys. Res.*, *107*(B6), 2110, doi:10.1029/2001JB000343.

Raddick, M. J., E. M. Parmentier, and D. S. Scheirer (2002), Buoyant decompression melting: A possible mechanism for intraplate volcanism, *J. Geophys. Res.*, *107*(B10), 2228, doi:10.1029/2001JB000617.

Schmeling, H. (2000), Partial melting and melt segregation in a convecting mantle, in *Physics and Chemistry of Partially Molten Rocks*, edited by N. Bagdassarov, D. Laporte, and A. B. Thompson, pp. 141–178, Kluwer Acad., Norwell, Mass.

Schubert, G., D. L. Turcotte, and P. Olson (2001), *Mantle Convection in the Earth and Planets*, 1st ed., Cambridge Univ. Press, New York.

Schutt, D. L., and C. E. Lesher (2006), Effects of melt depletion on the density and seismic velocity of garnet and spinel lherzolite, *J. Geophys. Res.*, *111*, B05401, doi:10.1029/2003JB002950.

Tackley, P. J., and D. J. Stevenson (1993), A mechanism for spontaneous self-perpetuating volcanism on the terrestrial planets, in *Flow and Creep in the Solar System: Observations, Modeling, and Theory*, edited by D. B. Stone and S. K. Runcorn, pp. 302–322, Kluwer Acad., Norwell, Mass.

Whitehead, J. A., H. J. B. Dick, and H. Schouten (1984), A mechanism for magmatic accretion under spreading centres, *Nature*, *312*, 146–148.

J. W. Hernlund, Department of Earth and Ocean Sciences, University of British Columbia, 6339 Stores Road, Vancouver, BC, Canada V6T 1Z4. (hernlund@gmail.com)

D. J. Stevenson, Division of Geological and Planetary Sciences, California Institute of Technology, 1200 E. California Blvd., Pasadena, CA 91125, USA.

P. J. Tackley, Institute for Geophysics, ETH-Zurich, Hönggerberg HPP L13, Schafmattstrasse 30, CH-8093 Zurich, Switzerland.